Boundary-Layer Meteorol
DOI 10.1007/s10546-015-0058-0

ARTICLE

Playa Soil Moisture and Evaporation Dynamics During the MATERHORN Field Program

Chaoxun Hang[1] · Daniel F. Nadeau[2] · Derek D. Jensen[1] · Sebastian W. Hoch[3] · Eric R. Pardyjak[1]

Received: 16 October 2014 / Accepted: 23 June 2015

Abstract We present an analysis of field data collected over a desert playa in western Utah, USA in May 2013, the most synoptically active month of the year, as part of the Mountain Terrain Atmospheric Modeling and Observations (MATERHORN) program. The results show that decreasing surface albedo, decreasing Bowen ratio and increasing net radiation with increasing soil moisture sustained a powerful positive feedback mechanism promoting large evaporation rates immediately following rain events. Additionally, it was found that, while nocturnal evaporation was negligible during dry periods, it was quite significant (up to 30 % of the daily cumulative flux) during nights following rain events. Our results further show that the highest spatial variability in surface soil moisture is found under dry conditions. Finally, we report strong spatial heterogeneities in evaporation rates following a rain event. The cumulative evaporation for the different sampling sites over a five-day period varied from ≈0.1 to ≈6.6 mm. Overall, this study allows us to better understand the mechanisms underlying soil moisture dynamics of desert playas as well as evaporation following occasional rain events.

Keywords Bare soil evaporation · Dry lake · Gravimetric method · Nocturnal evaporation · Spatial heterogeneity · Surface energy balance

1 Introduction

Drylands, defined as regions in which potential evapotranspiration exceeds annual precipitation, cover more than 40 % of the exposed earth surface (D'Odorico and Porporato 2006). Particularly in arid areas, where the average annual precipitation is less than 250 mm, soil

✉ Eric R. Pardyjak
pardyjak@eng.utah.edu

1 Department of Mechanical Engineering, University of Utah, Salt Lake City, UT 84112, USA

2 Department of Civil and Water Engineering, Université Laval, Quebec City, Canada

3 Department of Atmospheric Sciences, University of Utah, Salt Lake City, UT 84112, USA

Published online: 15 July 2015

moisture is known to be a key driver of eco-hydrological (D'Odorico and Porporato 2006) and meteorological (Seneviratne et al. 2010; Zhou and Geerts 2013; Massey et al. 2014) processes. Soil water content controls the partitioning of incoming energy at the surface into latent and sensible heat fluxes. Despite considerable efforts (Famiglietti et al. 1998, 2008; Teuling 2005; Tyler et al. 2006; Teuling et al. 2007; Vivoni et al. 2010; Ivanov et al. 2010; Mittelbach and Seneviratne 2012), because of the wide range of scales and processes involved, there are still knowledge gaps regarding spatial and temporal soil moisture dynamics in arid areas. A better understanding and parametrization of soil moisture content is necessary for predicting surface and boundary-layer variables, cloud formation, and atmospheric boundary-layer structure (Ookouchi et al. 1984; Avissar and Pielke 1989; Segal et al. 1989; Ek and Holtslag 2004; Zhou and Geerts 2013; Massey et al. 2014).

Temporal variations of soil moisture are controlled by a series of interactions at the land-atmosphere interface, such as precipitation and evapotranspiration, but also by water transport in the soil layer itself. Feedback mechanics involving soil moisture exist and can act to accelerate or decelerate water transport in the soil-vegetation-atmosphere continuum (Menenti 1984; Allison and Barnes 1985; Yechieli and Wood 2002; Warner 2004; Gowing et al. 2006; Tyler et al. 2006). For instance, when soil water content increases after a rainfall event, evaporation rates are enhanced and thus promote additional precipitation events (Koster and Suarez 2003). Even a small amount of rain can radically change the energy balance (Malek et al. 1990). In addition to increased water availability, wetter soils have a lower surface albedo, and thus more energy is available for evapotranspiration (Idso and Jackson 1975; Eltahir 1998; Zheng and Eltahir 1998; Schär et al. 1999). However, moist high salinity soils act to reduce evaporation by lowering the saturation vapour pressure (Warner 2004). These feedback mechanics are critical because they not only affect precipitation, but they also clearly affect the atmospheric boundary-layer structure (Rife et al. 2002; Zhou and Geerts 2013).

Soil water fluctuations are driven to a large extent by evapotranspiration at the land surface. In arid areas with very limited vegetation cover (such as desert playas—a remnant of an endorheic lake or an ephemeral lakebed), transpiration can be ignored and bare soil evaporation prevails. Following a rain event, bare soil evaporation has been shown to display two main stages based on theoretical studies (Philip 1957) and field experiments (Black et al. 1969; Parlange et al. 1992; Brutsaert and Chen 1995). In the first stage, when the soil is saturated, the evaporation rate is mostly controlled by the available energy and atmospheric drying power (i.e. wind speed, vapour pressure deficit, etc.) (Katul and Parlange 1992). In the second stage, the rate of evaporation is primarily limited by the soil moisture content and soil properties. Little is known about what controls the duration of each stage in the arid environment. In addition, recent studies have found that nocturnal evaporation could account for more than 10 % of the total daily evaporation (Burgess et al. 1998; Fisher and Baldocchi 2007; Dawson et al. 2007; Oishi et al. 2008). To the best of our knowledge, no previous studies have quantified the significance of nocturnal evaporation in arid areas. Given the large water vapour pressure deficits typically found at night (Novick et al. 2009), we hypothesize that nocturnal evaporation is significant over arid playas and should be quantified.

Studies on spatial patterns of soil moisture have proliferated in recent years originating from both meteorological and hydrological communities (Whitaker 1993; Scanlon and Goldsmith 1997; Lawrence and Hornberger 2007; Vivoni et al. 2008). As a result, several controlling factors of soil moisture spatial variability have been identified such as vegetation cover, soil texture, topography, and climate conditions (Famiglietti et al. 1998; Famiglietti 1999; Hupet and Vanclooster 2002; Teuling 2005; Brocca et al. 2007; Yeh et al. 1985). How-

ever, there does not appear to be a universal understanding of how spatial heterogeneity in soil water content varies with soil wetness. Some studies have reported less spatial heterogeneity in soil moisture under wet conditions (Famiglietti 1999; Hupet and Vanclooster 2002; Teuling 2005; Brocca et al. 2007), while other studies have reported the opposite (Hills and Reynolds 1969; Henninger et al. 1976; Bell et al. 1980; Famiglietti et al. 1998; Western and Grayson 1998; Teuling 2005). Moreover, some have reported greatest spatial heterogeneity in soil moisture under mid-range soil water contents (Owe et al. 1982; Albertson and Montaldo 2003; Famiglietti et al. 2008). In general, an understanding of soil moisture dynamics requires an analysis of sub-surface hydrology and boundary-layer processes (Entin et al. 2000; Brocca et al. 2007). Unfortunately, very few studies using this dual approach have focused on bare soils in arid areas (Williams et al. 2003).

The objectives of the paper are: (1) to determine how soil moisture affects the surface energy balance in an arid area; (2) to identify the key controlling mechanisms on evaporation after a rain event; (3) to explore the existence of nocturnal evaporation and investigate its main driving factors; (4) to characterize the spatial heterogeneity in soil moisture and evaporation rates. The analysis is supported by measurements made within the field experiment component of the Mountain Terrain Atmospheric Modeling and Observations (MATERHORN) program, designed to better understand atmospheric fluid dynamics across all scales over realistic mountainous terrain as well as under transient and steady conditions. The overall goal of MATERHORN project is to improve mountain weather forecasts by developing scientific tools to help identify leaps in predictability. More details can be found in Fernando and Pardyjak (2013) and Fernando et al. (2015).

2 Methods

2.1 Experimental Site Description

As part of the MATERHORN program, a spring field campaign was conducted from 1 to 31 May 2013 at the U.S. Army's Dugway Proving Ground (DPG), located about 137 km south-west of Salt Lake City, Utah. The DPG site is characterized by an arid climate with an annual cumulative precipitation of ≈100 mm and an annual cumulative evaporation of nearly 170 mm resulting in a net loss of water from the shallow water table (Malek 2003). The annual mean air temperature is ≈13.7 °C (Malek 2003). The terrain of the DPG site consists of sand dunes, salt flats and isolated hills surrounded by interconnected mountains, with sparse shrub steppe vegetation and very little human population. The main study area of interest here is a highly alkaline desert playa site (40°08′N, 113°27′W, 1296 m above mean sea level), which is mostly devoid of vegetation and characterized by a vast, barren and very flat surface, shallow water table and a heterogeneous soil moisture spatial distribution (Fig. 11a). The elevation variation on the playa is typically less than 1 m km^{-1}. The playa is ≈130 km long (north-south), and ≈65 km wide (east-west) and is located in the southern portion of the Great Salt Lake Desert.

The MATERHORN spring campaign contained ten Intensive Observation Periods (IOPs), during which extensive non-continuous datasets were collected (See Fernando et al. 2015 for details).

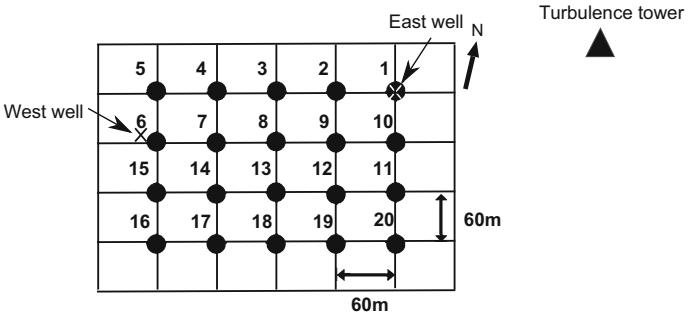

Fig. 1 Schematic illustrating the experiment layout (not to scale) with soil sampling sites (1–20) and the two wells monitoring the water table. The turbulence tower is located 200 m of the east well

2.2 Soil Moisture Content Sampling

2.2.1 Soil Sampling Transect

Soil moisture content was sampled at 20 sites evenly distributed on a 240 m × 180 m grid (Fig. 1). The grid size was selected to capture the typical length scale of wet and dry soil patches that are visible on the surface. Out of the 20 sampling sites, sites 1–17 were assigned to study the spatial heterogeneity of the playa soil. At these locations, soil from the surface layer (0–20 mm) and 50-mm layer (40–60 mm) were sampled. Here we assume that the spatial arrangement of wet and dry patches contained in our sampling grid is representative of the processes taking place at the playa scale. Sites 18–20 were used for mesoscale model validation purposes, which required extracting two soil cores from the layers 0 to 100 and 240 to 260 mm. Soil moisture was measured twice per IOP at sites 1–17, and once per IOP at sites 18–20, from the second IOP onwards (Table 1).

2.2.2 Moisture Content Sampling Method

Due to high salinity of the water in the playa soil, typical continuous moisture sampling probes such as reflectometers could not be used. As a result, volumetric water content (*VWC*) was measured directly using the gravimetric method (Johnson 1962). Soil samples were collected within a 1-m radius of each site by using a 25.4-mm gauge auger. The samples were taken sufficiently far from each other to prevent soil disruption throughout the field campaign. The soil samples were kept in pre-weighed tins immediately following extraction from the ground. The tins were sealed with electric tape and placed into plastic zipper bags. Once all of the samples were obtained, they were immediately weighed on-site before and after heating at 105 °C for at least 24 h. The precision of the scale was $\pm 10^{-5}$kg. The estimated uncertainty of *VWC* was found to be $\pm 0.012\,\mathrm{m}^3\,\mathrm{m}^{-3}$. In order to convert from mass to volume, the density of the water and soil were both measured in the field using the recommended USDA soil quality test kit guide (USDA 1999). The volumetric water content of each soil sample was taken as the ratio of the volume of the water inside of the soil to the volume of the dry soil. To characterize the spatial heterogeneity statistically, mean and standard deviations were computed over all sampling results for each IOP (e.g. mean surface-layer *VWC* during IOP2 was the average over all surface samples from the 17 sites during IOP2). The density of the saline water in the soil was found to be $\approx$1080 kg m^{-3} and the bulk density of the soil was 1426.2 kg m^{-3}.

Table 1 Surface (0–20 mm) temporal variability of playa soil moisture during the experimental period

IOP	Sampling time		*VWC* (m^3 m^{-3})		
	Start–final (MST)		Mean	Min/Max	Std
2	May 4	1411–1642	0.22	0.05/0.33	0.08
	May 5	0937–1026			
3	May 7	1353–1510	0.24	0.08/0.34	0.08
	–				
4	May 11	1200–1238	0.20	0.06/0.32	0.10
	May 12	0414–0604			
5	May 13	1845–1926	0.20	0.06/0.31	0.07
	May 14	0937–1026			
6	May 16	2219–0037	0.21	0.05/0.35	0.11
	–				
7	May 20	1325–1455	0.34	0.16/0.42	0.05
	May 21	0441–0526			
8	May 22	1351–1512	0.30	0.15/0.38	0.06
	May 23	0615–0700			
9	May 25	1028–1110	0.27	0.04/0.36	0.09
	May 25	0724–0811			
10	May 30	1904–1932	0.33	0.28/0.36	0.02
	–				

Std standard deviation

2.3 Other Measurements

To determine the evaporation and corresponding atmospheric variables at the playa site, we use 20-Hz data from a 28-m turbulence flux tower, which ran nearly continuously from 2 May to 5 June 2013. The tower was instrumented at six levels (0.6, 2.0, 5.3, 10.4, 19.4, 25.5 m) with Campbell Scientific, Inc. CSAT3 sonic anemometer/thermometers (Logan, UT) and HMP45C temperature/relative humidity sensors (Vaisala, Vantaa, Finland). Two EC150 CO_2/H_2O open-path gas analyzers (Campbell Scientific, Inc., Logan, UT) were deployed at 2.0 and 10.4 m above the surface. The eddy-covariance technique was applied to obtain sensible and latent heat fluxes using averaging periods of 30 min. More details on the turbulence flux corrections and quality control can be found in Jensen et al. (2015). The random flux uncertainty was estimated based on Lenschow et al. (1994). Here, we purposely did not exclude nocturnal data segments characterized by weak or 'insufficient' mechanical mixing. Indeed, given the closure of the surface energy balance at night (see Fig. 3), we have no indication that the latent heat fluxes are underestimated. The estimations of nocturnal evaporation reported in Sect. 3.2 are, in the worst case, conservative.

Thermal property sensors (TP01, Hukseflux, Delft, the Netherlands) were installed at a depth of 50 and 250 mm to measure soil thermal conductivity, soil thermal diffusivity, and volumetric heat capacity. The sub-surface heat flux at 50 mm depth was measured with self-calibrating heat-flux plates (HFP-SC, Hukseflux, the Netherlands). The ground heat flux at the surface was then calculated as the sum of the average measured ground heat flux at 50-mm depth (flux plate measurements) and the heat storage change in the 0 to 50-mm soil layer. The heat storage was calculated using the direct measurements of thermal heat capacities at 50 mm below the surface and soil temperatures at depths of 10, 25, and 50 mm. Given

the low permeability of the soil, advective heat transport by rain infiltration was neglected. The individual shortwave and longwave components of the surface radiation balance were measured with up- and down-facing pyranometers and pyrgeometers (CMP21 and CGR4, Kipp & Zonen, the Netherlands) mounted horizontally 2 m above ground.

Finally, two Solinst Model 3001 Levelogger (Ontario, Canada) probes were installed at the field site (marked with an × in Fig. 1) to measure water table depth as it is a critical hydrological variable for dry lake beds (Tyler et al. 2006).

2.4 Soil Textures

As shown in Table 2, the study site is characterized by tremendous spatial variability in soil textures. In the top 250 mm, the soil texture is clay, silty clay or silty clay loam. In the surface soil layer (0–20 mm), the percentage of sand varies from 1 to 22 %, whereas silt varies from 24 to 55 % and clay from 41 to 62 %. All soil texture data were determined with the hydrometer method (Day 1965). Malek (2003) reported the surface salt content at a site ≈250 m to the north-east of the present measurement site, finding a soil electrical conductivity of 140 dS m^{-1} and a predominance of sodium, thereby explaining the white tinted surface soil colour.

3 Results and Discussion

3.1 Brief Climatology

Figure 2 shows a summary of basic hydrological and meteorological conditions during the field campaign at the playa site. Figure 2a reveals two main rain events in May 2013 (rainfall data obtained from a nearby automated weather station, 40°197′N, 113°167′W, 1299 m above mean sea level). The first occurred on 17–18 May 2013, with a cumulative rainfall of 15.8 mm, whereas the second took place on 28 May 2013, with a total rainfall of 10.2 mm. Figure 2a also shows the water-table depth fluctuations for part of the experimental period. Apart from a weak daily cycle possibly attributable to evaporative losses, we note two different time scales in the water table response to rainfall events. Following the first rain event, it took roughly 4 days for the water table to start rising, while for the second event it took only a day. One potential reason for these two different time scales is the antecedent soil moisture conditions. The last rain event before 17 May 2013 was 20 April 2013, allowing 30 days for soil to dry out. However, the second rain event occurred only 10 days after the first event, so, the antecedent soil moisture during the second event was higher than for the first rain event, which led to a more rapid response to the water table depth. Figure 2b shows the evolution of air temperature and wind speed throughout the experimental period, with air temperature varying between 1.8 and 34.1 °C, with an average of 17.4 °C. The mean 2-m wind speed was 4 m s^{-1} and reached a maximum of 17 m s^{-1} on 23 May at night. Figure 2c shows the evaporation rate measured using the eddy-covariance technique at the site from 2 May to 5 June 2013. The mean daily cumulative evaporation before 17 May 2013 was about 0.3 ± 0.2 mm. We note an increase in evaporation rates after the first rain event, followed by a sharp decay (see following section). The peak evaporation rates following the two rain events were 5.9 mm day^{-1} (±0.4 mm day^{-1}) and 8.3 mm day^{-1} (±0.3 mm day^{-1}) respectively. These events are discussed thoroughly in Sect. 3.2. Note that the cumulative evaporation for the entire experimental period was 19.3 mm (±1.5 mm) (73 % of the rainfall received during the campaign). The monthly averaged evaporation rate is 0.69 mm day^{-1}, which is consistent with the annual mean evaporation rate of 0.46 mm day^{-1} reported by Malek (2003).

Table 2 Playa soil texture analysis for Site 1–Site 17 following the USDA classification system (Soil Survey Staff 1999) as well as basic *VWC* statistics

Site number	Texture	Sand (%)	Silt (%)	Clay (%)	*VWC* (m^3m^{-3})		
					Mean	Min/Max	Std
1	SC	9	45	46	0.29	0.19/0.35	0.04
1 (40–60 mm)	SC	0	56	44	–	–	–
1 (200–250 mm)	SC	0	51	49	–	–	–
2	C	10	36	54	0.25	0.04/0.40	0.11
3	SC	1	48	51	0.19	0.05/0.34	0.09
4	C	16	30	54	0.20	0.07/0.32	0.09
5	C	14	31	55	0.20	0.06/0.33	0.09
6	SC	9	40	51	0.33	0.29/0.38	0.03
7	SC	1	55	44	0.29	0.17/0.37	0.06
8	SC	7	52	41	0.32	0.25/0.37	0.03
9	C	10	38	52	0.21	0.06/0.34	0.09
10	C	10	36	54	0.23	0.06/0.33	0.10
11	C	22	37	41	0.31	0.22/0.42	0.06
12	C	17	27	56	0.19	0.08/0.34	0.09
13	C	14	24	62	0.26	0.10/0.38	0.09
14	C	20	40	41	0.30	0.14/0.42	0.07
15	C	15	32	54	0.27	0.18/0.36	0.06
16	C	10	34	56	0.29	0.12/0.41	0.10
16 (40–60 mm)	SCL	16	44	40	–	–	–
16 (200–250 mm)	SCL	11	51	38	–	–	–
17	C	16	30	54	0.23	0.06/0.39	0.11
Mean		11.8	37.3	50.9	–	–	–
Min/Max		1/22	24/55	41/62			

Unless specified, the reported soil texture and *VWC* are averaged over the entire experimental period and are reported for the top 20-mm soil layer
SC: silty clay, C: clay, SCL: silty clay loam

3.2 Atmosphere–Soil Moisture Dynamics

Figure 3 shows the full surface energy balance around the first rain event, which occurred on 17–18 May 2013 (see Fig. 2a). Before the rain event, the peak value of net radiation was about 400 Wm^{-2}. During and after the rain event, the maximum net radiation exceeded 500 Wm^{-2} and continued to do so for at least the next 3 days. As surface soil moisture increases following precipitation events, the surface albedo decreases, leading to reduced outgoing shortwave radiation flux densities and an increase in net radiation, especially under less cloudy conditions. Furthermore, as the most synoptically active month of the year, most of the data were obtained under cloudy conditions. Figure 3 also shows that the sensible heat flux decreased by a factor of ≈2 during the rain event. After approximately one day, the sensible heat flux returned to its pre-rainfall values. The nighttime sensible heat flux is very small (near zero), indicating near-neutral surface layer conditions on certain days (see also Jensen et al. 2015). As required, the latent heat fluxes show the same behaviour observed with

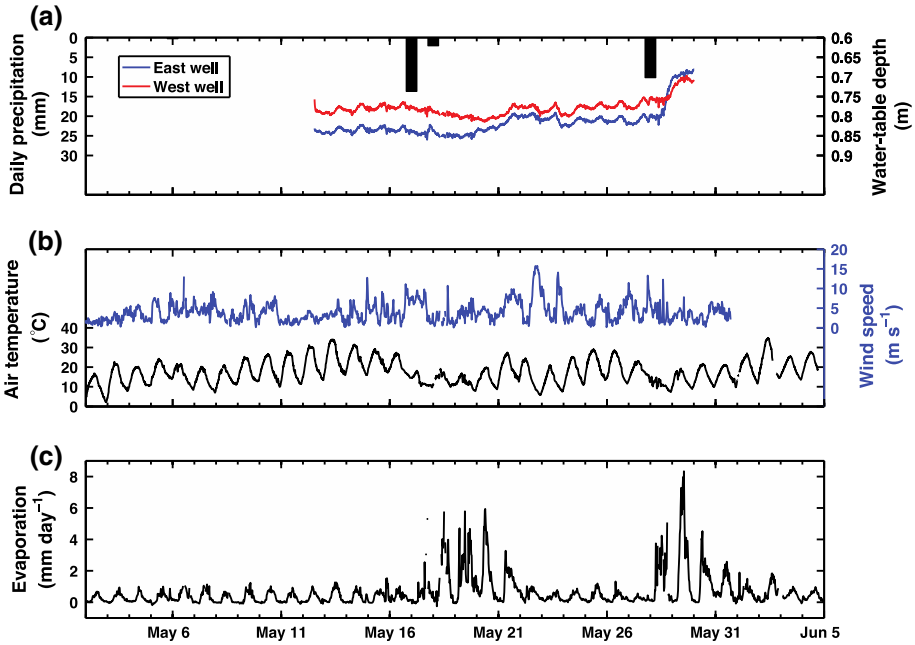

Fig. 2 **a** Daily precipitation and water-table level during the experimental period. **b** 5-min averages of air temperature and wind speed at 2 m above ground from the flux tower. **c** 30-min averages of evaporation rates measured 10 m above ground. *Error bars* are not included for readability

the evaporation rate shown in Fig. 2c. The magnitude of the ground heat flux increases during the rainfall and reaches its maximum value on 20 May 2013, partly because of variations in soil thermal conductivity. Indeed, before the rain event, the thermal conductivity was 0.71 W $(\mathrm{mK})^{-1}$ and immediately after, it increased to 0.85 W $(\mathrm{mK})^{-1}$. Due to the fact that the soil in this studied area is rich in clay, the advective transport of heat is very small and is thus neglected as previously mentioned. The magnitude of the daytime residual heat flux is about 100 Wm^{-2} before the rain, and increases to 200 Wm^{-2} for a brief period. As can be seen in Fig. 3, there are missing data, both due to the rain event and a brief power outage.

Several studies have reported exponential decay of evapotranspiration following a rain event (Williams and Albertson 2004; Teuling et al. 2006), and in order to relate evaporation to the soil moisture dynamics, the model presented in Teuling et al. (2006) is applied here. The model has a basic simplified terrestrial water balance under the assumptions that there is no rainfall and no runoff,

$$\frac{\mathrm{d}S(t)}{\mathrm{d}t} = -E(t), \tag{1}$$

and assumes evaporation E is proportional to the available soil moisture storage S with proportionality constant c. Then, Eq. 1 can be integrated from t_0 to t and written as,

$$E(t) = E_0 \exp\left(\frac{-(t - t_0)}{\lambda}\right), \tag{2}$$

where E_0 is the evaporation at $t = t_0$ (t_0 is specified as the first day following the rain event) and $\lambda = 1/c$ is a time scale controlling the temporal evolution of evaporation. If the evaporation rate is plotted as function of time on a semi-log plot (Fig. 4), E_0 is given by the

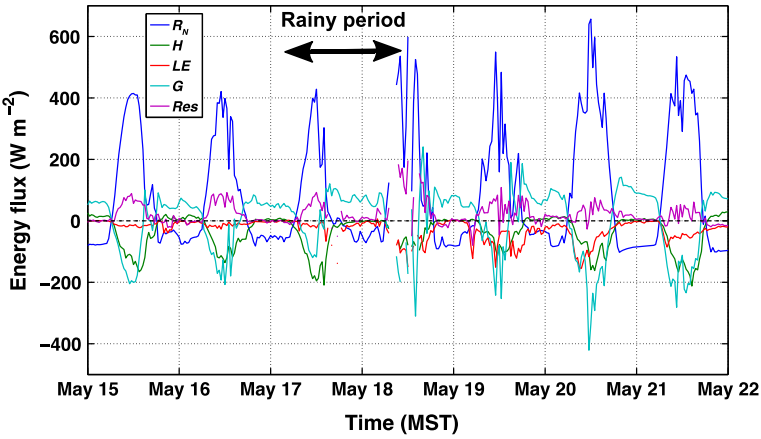

Fig. 3 Surface energy balance ($R_N + H + LE + G = Res$) for a six-day period centered on the first rain event (17 May 2013). Energy fluxes shown are 30-min averages (R_N net radiation, H sensible heat flux, LE latent heat flux, G ground heat flux, Res residual energy). More details on the surface energy balance can be found in Hoch et al. (2013, 2014)

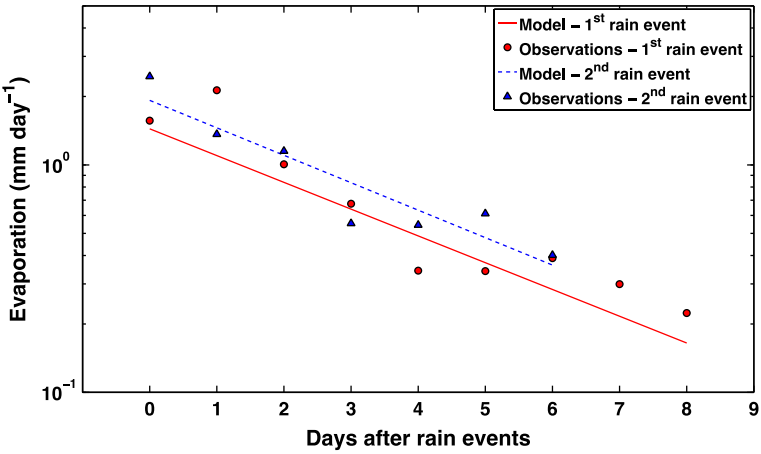

Fig. 4 Daily evaporation at the field site following two rain events. The model evaluated here is the one from Teuling et al. (2006) (see Eq. 2). The first rain event took place on 17–18 May 2013 and the second on 28 May 2013

intercept with the ordinate obtained using a linear regression. In order to connect the time scale λ to the soil moisture dynamics, a storage term S_0 is defined as soil moisture depleted following a complete drydown ($t \to \infty$),

$$S_0 = \int_{t_0}^{\infty} E(t)\mathrm{d}t = \lambda E_0 \tag{3}$$

In their study, Teuling et al. (2006) report λ and S_0 values for a wide range of surface types and climate conditions. During the MATERHORN field experiment, the mean e-folding time was found to be $\lambda = 3.64$ days, and $S_0 = 6.12$ mm, values that are much smaller than those reported in Teuling et al. (2006). In fact, the minimum λ and S_0 from their Table 2 are 12.4 days and 28.1 mm respectively. We believe that the short e-folding time is due to the high

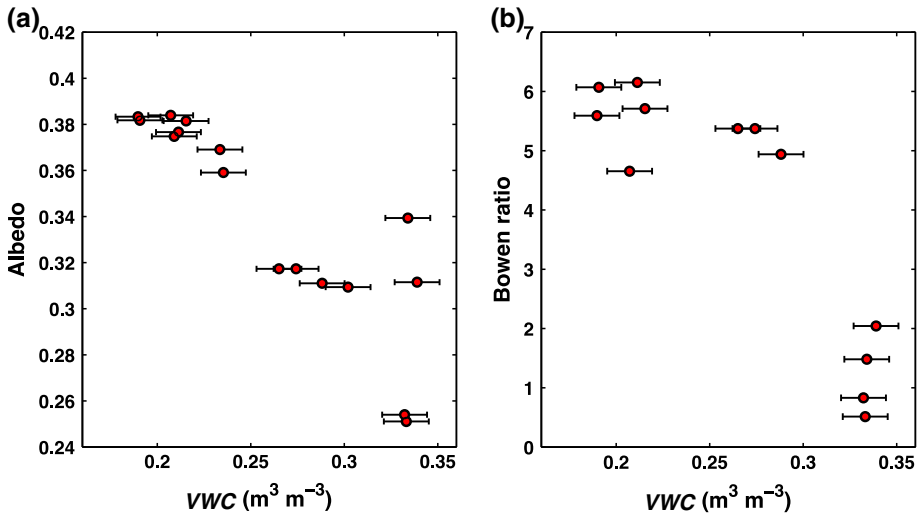

Fig. 5 *Left* Average daytime surface albedo versus mean volumetric water content (*VWC*) for each IOP. *Right* Average daytime Bowen ratio versus mean volumetric water content for each IOP

atmospheric drying demand at the playa site, to the fine texture of the soil retaining rainwater close to the surface, and to the existence of positive feedback mechanisms promoting fast surface drying after a rain event. On the other hand, the low storage volume is possibly a result of the soil properties and shallow water table position at the field site.

As shown in Table 2, the surface soil texture at the playa is mainly clay, which has a very low permeability due to its fine texture. Furthermore, clay rich soil has a relatively high water capacity. As a result, water is kept near the surface after the rain events, which promotes large evaporation rates.

As a starting point to investigate processes responsible for the unusually rapid surface drying following a rain event, we focus on two key determinants of the energy budget: the playa surface albedo and Bowen ratio. Figure 5a presents variations of surface albedo as a function of *VWC* in the surface layer, where we see that the surface albedo increases by up to a factor of 1.5 in response to a drying surface. In terms of energy fluxes, this reduction of 0.13 in surface albedo translates into an increase of 80 W m^{-2} given the typical conditions at the site. Figure 5b shows the relationship between the daytime Bowen ratio and surface soil moisture, with the Bowen ratio taken as the ratio of the mean daytime sensible heat flux to latent heat flux. The Bowen ratio varies greatly, from ≈ 6 to 0.5 as *VWC* in the surface layer increases. The variation of Bowen ratio under dry and medium soil moisture conditions ($VWC \approx 0.18$–$0.29\,m^3\,m^{-3}$) is relatively small, but under wet conditions ($VWC \approx 0.29$–$0.34\,m^3\,m^{-3}$) it increases sharply from about 5 to 0.5, i.e. by a factor of 10. In essence, Fig. 5 shows that both surface albedo and Bowen ratio decrease with increasing surface wetness, a well-known relationship.

Given that there is more energy available at the surface under wet conditions, one needs to investigate how this excess energy is redistributed. Figure 6 shows sensible (H), latent (LE) and ground (G) heat fluxes normalized by net radiation (R_N). The 30-min averaged data of all the heat fluxes are integrated over a 24-h period, which imply values of the daily total heat transfer. The daily total net radiation increases from 6.2 to 12.5 MJ m^{-2} with increasing wetness. Figure 6a illustrates that the integrated sensible heat flux has a slightly increasing

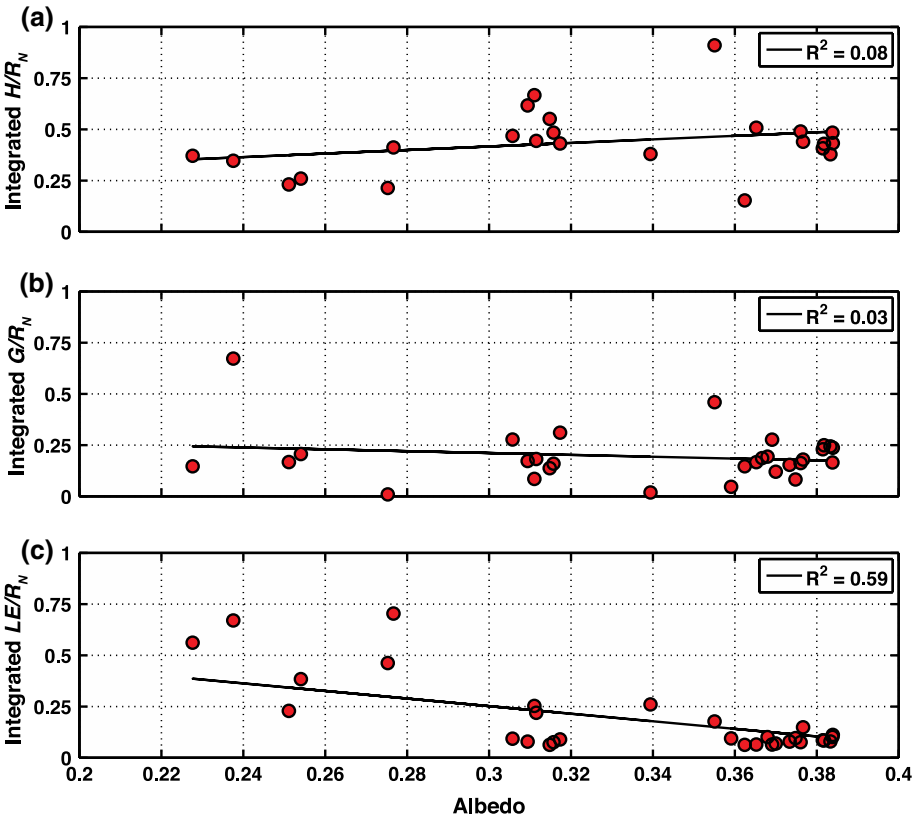

Fig. 6 **a** Integrated sensible heat flux over 1 day normalized by daily-averaged net radiation versus daily averaged surface albedo. **b** Integrated ground heat flux over a day normalized by daily-averaged net radiation versus daily-averaged surface albedo. **c** Integrated latent heat flux over a day normalized by daily-averaged net radiation versus daily-averaged surface albedo

trend with increasing albedo. Under relatively low-albedo conditions (0.22–0.31), integrated H/R_{N} increases from about 0.2 to 0.5 and then levels off when surface albedo is greater than 0.32. This indicates that the temperature difference between the soil surface and the overlying air increases under moist low-albedo conditions. Figure 6b does not show any clear relation between the integrated G and albedo as indicated by the very small correlation coefficient. This can be explained by the balance of increasing soil thermal conductivity and decreasing temperature difference when the albedo becomes smaller (greater soil moisture content). Figure 6c shows a decreasing trend of integrated LE/R_{N} as albedo increases. The integrated LE decreases from ≈0.6 to 0.1 under small albedo conditions, and then appears to plateau when surface albedo exceeds 0.36. In summary, when the soil moisture content increases (i.e. after a rain event), the surface albedo decreases and the additional energy is used to evaporate more water and thus accelerate surface drying.

We hypothesize that nocturnal evaporation is another factor behind the positive surface drying feedback mechanism. Figure 7 shows that nocturnal evaporation (obtained from the eddy-covariance measurements) can account for up to 30 % of the cumulative daily evaporation, although it is usually in the range 0–10 %. Note that this has implications for traditional radiation-based evaporation relations such as that of Priestley and Taylor (1972), which

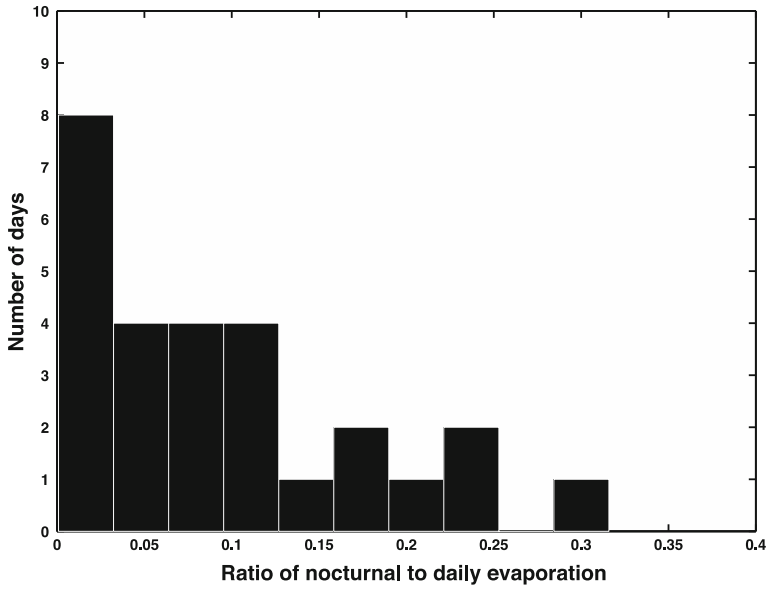

Fig. 7 Histogram of the ratio of nocturnal to daily cumulative evaporation for the full experimental period

assume that nighttime evaporation is non-existent. The use of such relations over long time periods could lead to an underestimation of the actual water vapour transfer.

To investigate the driving process related to nocturnal evaporation, Fig. 8 shows the cumulative nocturnal evaporation versus the mean atmospheric drying power (a–c) and surface soil moisture content (d). Note that the *VWC* data are available exclusively during the IOP periods, which focused on daytime conditions. Thus, Fig. 8d represents nighttime evaporation versus the corresponding *VWC* values for the equivalent day. Negative evaporation indicates that on certain days, weak condensation occurs, although these values may result from random flux errors. There is no clear relation between cumulative nocturnal evaporation and atmospheric drying demand. In most cases, no matter how the atmospheric dying power changes, total nighttime evaporation only varies slightly from zero to 0.1 mm (Fig. 8a–c). However, nocturnal evaporation is positively correlated with *VWC* (Fig. 8d); therefore, in arid areas devoid of vegetation such as playas, nocturnal evaporation is essentially limited by water availability, as one would expect.

3.3 Spatial Heterogeneity of Soil Moisture and Evaporation

Figure 9 shows the spatial standard deviation of *VWC* values in the soil surface layer computed with data from all IOPs at sites 1–17. In the surface soil layer, the spatial heterogeneity increases as the soil becomes drier. Under the driest surface conditions, the coefficient of variation is 50 %, while under the wettest conditions it decreases to 14 %. Yeh et al. (1985) were the first to postulate that increased heterogeneities under dry conditions were due to variations in soil texture, as is likely the case here. This surface variability was evident in visual observations of persistent moist and dry regions throughout the playa (Fig. 11a). However, at greater soil depths, less heterogeneity is observed until eventually the soil becomes saturated. Thus, there is no clear relation between mean soil moisture and its standard deviation in the 50-mm layer. As expected, a larger range of soil moisture conditions was found in the surface

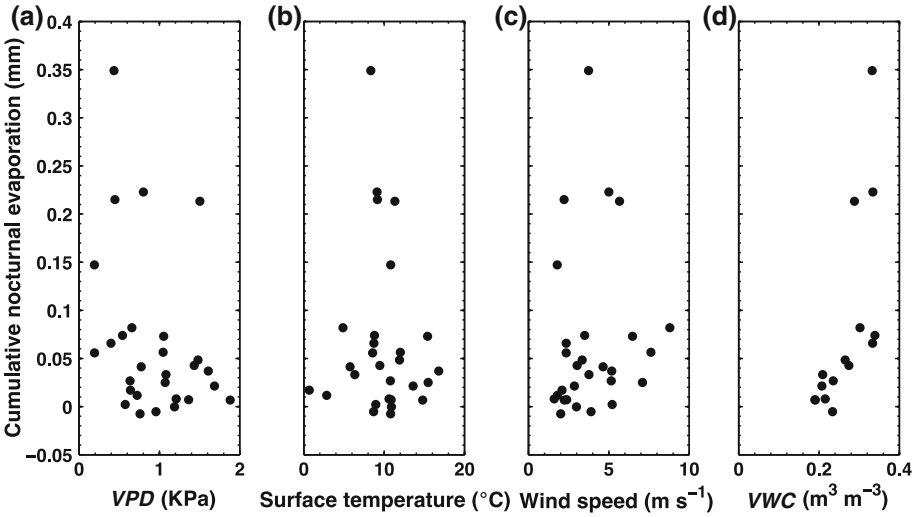

Fig. 8 Nocturnal cumulative evaporation (mm) versus: **a** vapour pressure deficit (*VPD*); **b** soil surface temperature; **c** wind speed measured 2 m above ground; **d** surface volumetric water content (*VWC*)

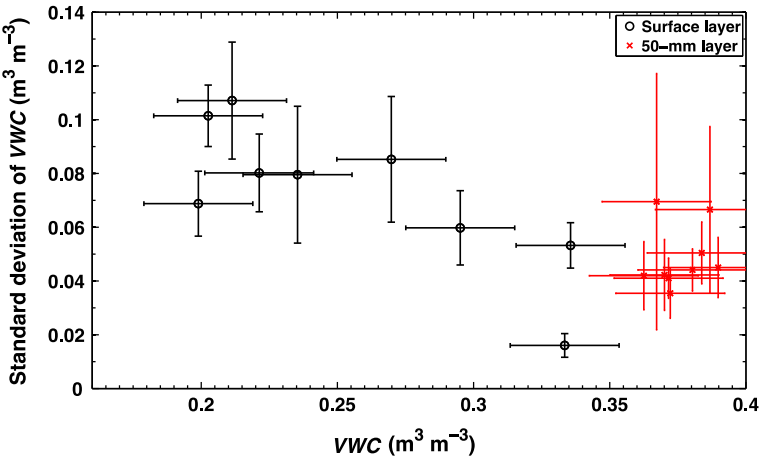

Fig. 9 Standard deviation of volumetric water content in the surface soil layer and 50-mm soil layer versus mean volumetric water content. Standard deviation of *VWC error bars* represent 95 % confidence intervals calculated with a jackknife resampling algorithm (Tukey 1958). *VWC error bars* represent the mean error of soil sampling

layer, where it varied from 0.20 to 0.34 $m^3\ m^{-3}$. In the 50-mm layer, *VWC* covered the range 0.36–0.39 $m^3\ m^{-3}$.

One would expect spatial heterogeneity in soil moisture to translate into heterogeneity in evaporation rates. To investigate this, we used the soil moisture depletion technique (Johnston et al. 1969) at each of our 17 sampling sites with soil water profiles obtained, by solving Richards equation with a simple finite difference model (Clapp and Hornberger 1978; McCumber 1980; Shingleton 2010 for more detail on the model). As the top boundary condition, we used our surface soil moisture measurements, whereas for the bottom boundary

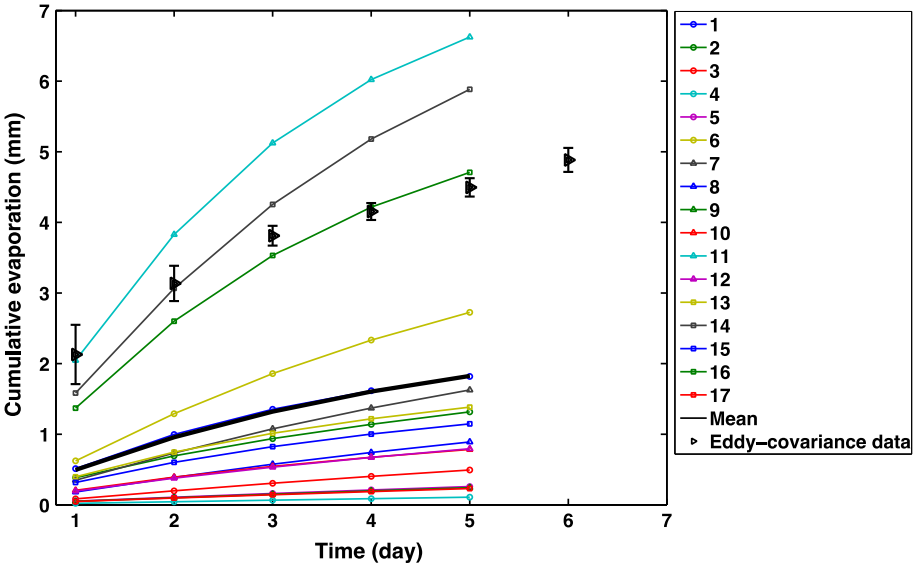

Fig. 10 Cumulative evaporation for each of the 17 soil sampling sites as determined from the soil depletion method and the eddy-covariance measurements. *Error bars* on eddy-covariance data represent the estimated random errors of daily evaporation

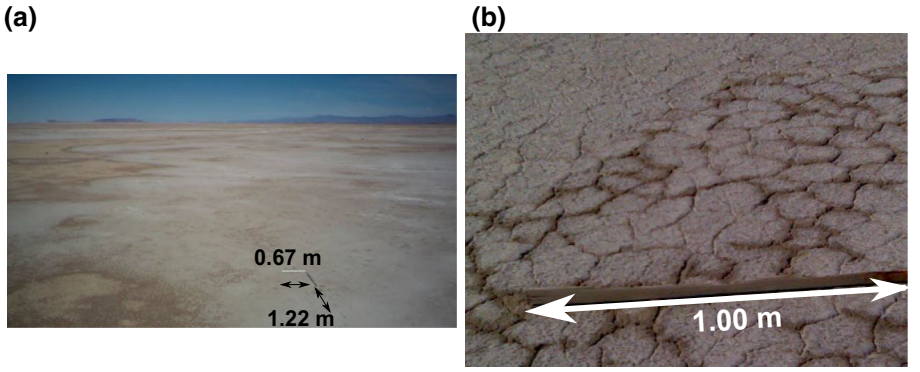

Fig. 11 **a** Large-scale visible photograph of the desert playa (19 June 2014 1335 MST); **b** small-scale visible photograph showing desiccation cracks (23 July 2014 1530 MST)

conditions (0.8 m below the surface) we assumed a saturated soil with $VWC = 0.46\,\mathrm{m^3\,m^{-3}}$. We validated the model by comparing the variations of 50-mm soil moisture after the rain event on May 17–18. Although this is far from an exhaustive validation, the differences between observational and modelled values were relatively small and considered sufficiently good to proceed with the analysis. Figure 10 shows substantial variability in evaporation rates among the 17 sampling sites. The cumulative evaporation on the first day after the last rain event varies from ≈0 to 2.0 mm. However, the values of total evaporation after 5 days changes from ≈0.1 to ≈6.6 mm, which indicates strong heterogeneity over these 17 sites. As expected, most of the sites with smaller-than-average evaporation are usually relatively dry ($VWC < 0.2\,\mathrm{m^3\,m^{-3}}$) and vice versa. In essence, Fig. 10 illustrates the underlying spatial

variability in evaporation rates, which an 'integrated' measurement approach such as the eddy-covariance method is unable to detect.

As highlighted by Brutsaert (1998), spatial heterogeneity in soil moisture (and thus water vapour fluxes) exists at multiple scales. Figure 11 shows visible photographs of the playa site at two scales. At large scales (Fig. 11a), clear dry (brown) and wet (white) patches are found and are likely associated with sharp local gradients in evaporation rates. Heterogeneity is also found at small scales (Fig. 11b), where water vapour is evacuated through small desiccation cracks. This illustrates that even under a priori homogeneous surfaces, spatial heterogeneity has to be taken into account.

4 Conclusions

This study focuses on mechanisms controlling desert playa soil moisture dynamics as well as evaporation following occasional rain events. The analysis is based on observational data collected as part of the MATERHORN program in May 2013. This month is typically the most synoptically active month of the year, and while there were only two significant rain events during the month, total precipitation (25 mm) did exceed cumulative evaporation (19 mm). Hence, the month was relatively wet compared to the annual averages where evaporation exceeds precipitation.

Regarding the temporal variability of soil moisture, a fast positive feedback mechanism promoting surface drying after precipitation events was observed. Following rainfall, surface albedo and Bowen ratio decreased from 0.38 to 0.25 and from 6 to 0.5 respectively, while net radiation increased by 25 %. The evaporation rate reached its maximum value one day after the rain event, and then decayed exponentially. The associated e-folding time scale is much smaller than values previously reported in the literature. An additional contributing factor to the positive drying feedback mechanism is nocturnal evaporation. Furthermore, the clay soil at the playa site is characterized by low permeability and a relatively large water holding capacity, which holds water near the surface and is available for evaporation. On several nights following rain events, the ratio of nocturnal to daily cumulative evaporation reached up to 30 %. Near-surface volumetric water content has a bigger impact than they do vapour pressure deficit, surface temperature and wind speed.

High spatial variability of surface soil moisture and soil texture was also investigated on an experimental grid. The spatial heterogeneity was found to be significant in the top 20-mm layer, with a *VWC* standard deviation of $0.07\,m^3\,m^{-3}$, and negligible deeper into the soil, with a *VWC* standard deviation of $0.05\,m^3\,m^{-3}$. Cumulative evaporation after rain events shows the presence of strong heterogeneity in evaporation rates under wet soil conditions (relatively low variability). The total evaporation after 5 days varied from $\approx$0.1 to $\approx$6.6 mm. Some evidence of a positive feedback mechanism over a desert playa site was observed, and additionally we also identified strong spatial heterogeneity at different scales for playa sites.

Acknowledgments This research was funded by the Office of Naval Research Award #N00014-11-1-0709, Mountain Terrain Atmospheric Modeling and Observations (MATERHORN) Program. The authors thank Daniel Alexander for his help with the finite difference model of the Richard's equation used to compute soil moisture profiles. The authors are also grateful to Dr. Dragan Zajic, John Pace and Nipun Gunawardena whose contributions were critical to the success of the field measurements. We are also extremely grateful for all of the help in the field, and the scientific insight provided by the MATERHORN team, especially Prof. H.J.S. Fernando.

References

Albertson JD, Montaldo N (2003) Temporal dynamics of soil moisture variability: 1. Theoretical basis. Water Resour Res 39:1274

Allison GB, Barnes CJ (1985) Estimation of evaporation from the normally "dry" Lake Frome in South Australia. J Hydrol 78(3):229–242

Avissar R, Pielke RA (1989) A parameterization of heterogeneous land surfaces for atmospheric numerical models and its impact on regional meteorology. Mon Weather Rev 117:2113–2136

Bell KR, Blanchard BJ, Schmugge TJ, Witczak MW (1980) Analysis of surface moisture variations within large-field sites. Water Resour Res 16:796–810

Black TA, Gardner WR, Thurtell GW (1969) The prediction of evaporation, drainage, and soil water storage for a bare soil. Soil Sci Soc Am J 33:655

Brocca L, Morbidelli R, Melone F, Moramarco T (2007) Soil moisture spatial variability in experimental areas of central Italy. J Hydrol 333:356–373

Brutsaert, W. (1998). Landsurface water vapor and sensible heat flux: Spatial variability, homogeneity, and measurement scales. Water Resour Res 34(10), 2433–2422

Brutsaert W, Chen D (1995) Desorption and the two stages of drying of natural tallgrass prairie. Water Resour Res 31:1305–1313

Burgess SSO, Adams MA, Turner NC, Ong CK (1998) The redistribution of soil water by tree root systems. Oecologia 115:306–311

Clapp R, Hornberger G (1978) Empirical equations for some soil hydraulic properties. Water Resour Res 14:601–604

D'Odorico P, Porporato A (2006) Dryland ecohydrology. Springer, Dordrecht, 341 pp

Dawson TE, Burgess SSO, Tu KP, Oliveira RS, Santiago LS, Fisher JB, Simonin KA, Ambrose AR (2007) Nighttime transpiration in woody plants from contrasting ecosystems. Tree Physiol 27:561–575

Day PR (1965) Particle fractionation and particle-size analysis. In: Black CA (ed) Methods of soil analysis, part 1. American Society of Agronomy No. 9, Madison, pp 545–567

Ek MB, Holtslag AAM (2004) Influence of soil moisture on boundary layer cloud development. J Hydrometeorol 5:86–99

Eltahir E (1998) A soil moisture-rainfall feedback mechanism 1. Theory and observations. Water Resour Res 34:765–776

Entin JK, Robock A, Vinnikov KY, Hollinger SE, Liu S, Namkhai A (2000) Temporal and spatial scales of observed soil moisture variations in the extratropics. J Geophys Res 105:11865

Famiglietti JS (1999) Ground-based investigation of soil moisture variability within remote sensing footprints during the southern great plains 1997. Water Resour Res 35:1839–1851

Famiglietti JS, Rudnicki JW, Rodell M (1998) Variability in surface moisture content along a hillslope transect: Rattlesnake Hill, Texas. J Hydrol 210:259–281

Famiglietti JS, Ryu D, Berg AA, Rodell M, Jackson TJ (2008) Field observations of soil moisture variability across scales. Water Resour Res 44:W01423

Fernando HJS, Pardyjak ER (2013) Field studies delve into the intricacies of mountain weather. Eos Trans Am Geophys Union 94:313–320

Fernando HJS, Pardyjak ER, Di Sabatino S, Chow FK, De Wekker SFJ, Hoch SW, Hacker J, Pace JC, Pratt T, Pu Z, Steenburgh JW, Whiteman CD, Wang Y, Zajic D, Balsley B, Dimitrova R, Emmitt GD, Higgins CW, Hunt JCR, Knievel JC, Lawrence D, Liu Y, Nadeau DF, Kit E, Blomquist BW, Conry P, Coppersmith RS, Creegan E, Felton M, Grachev A, Gunawardena N, Hang C, Hocut CM, Huynh G, Jeglum ME, Jensen D, Kulandaivelu V, Lehner M, Leo LS, Liberzon D, Massey JD, McEnerney K, Pal S, Price T, Sghiatti M, Silver Z, Thompson M, Zhang H, Zsedrovits T (2015) The MATERHORN—unraveling the intricacies of mountain weather. Bull Am Meteorol Soc. doi:10.1175/BAMS-D-13-00131.1

Fisher J, Baldocchi D (2007) What the towers don't see at night: nocturnal sap flow in trees and shrubs at two AmeriFlux sites in California. Tree Physiol 27:597–610

Gowing JW, Konukcu F, Rose DA (2006) Evaporative flux from a shallow watertable: the influence of a vapour–liquid phase transition. J Hydrol 321(1–4):77–89

Henninger DL, Petersen GW, Engman ET (1976) Surface soil moisture within a watershed—variations, factors influencing, and relationship to surface runoff. Soil Sci Soc Am J 40:773

Hills RC, Reynolds SG (1969) Illustrations of soil moisture variability in selected areas and plots of different sizes. J Hydrol 8:27–47

Hoch SW, Jensen D, Pardyjak ER, Whiteman CD, Fernando HJ (2013) Surface energy balance observations during MATERHORN. In: 32nd International Conference on Alpine Meteorology, Kranjska Gora, Slovenia, 3–7 June 2013

Hoch SW, Jensen D, Massey JD, Pardyjak ER, Fernando HJS (2014) Surface energy balance observations during MATERHORN. In: 16th American Meteorological Society Conference on Mountain Meteorology, San Diego, CA, 18–22 Aug 2014

Hupet F, Vanclooster M (2002) Intraseasonal dynamics of soil moisture variability within a small agricultural maize cropped field. J Hydrol 261:86–101

Idso S, Jackson R (1975) The dependence of bare soil albedo on soil water content. J Appl Meteorol Climatol 14:109–113

Ivanov VY, Fatichi S, Jenerette GD, Espeleta JF, Troch Pa, Huxman TE (2010) Hysteresis of soil moisture spatial heterogeneity and the "homogenizing" effect of vegetation. Water Resour Res 46:W09521

Jensen DD, Nadeau DF, Hoch SW, Pardyjak ER (2015) Observations of near-surface heat flux and temperature profiles through the early evening transition over contrasting surfaces. Boundary-Layer Meteorol. doi:10.1007/s10546-015-0067-z

Johnson A (1962) Methods of measuring soil moisture in the field. US Government Printing Office, Washington, 25 pp

Johnston RS, Doty RD, Tew RK (1969) Soil moisture depletion and estimated evapotranspiration on Utah mountain watershed. USDA Forest Service – Research Papers International-67

Katul GG, Parlange MB (1992) Estimation of bare soil evaporation using skin temperature measurements. J Hydrol 132:91–106

Koster R, Suarez M (2003) Observational evidence that soil moisture variations affect precipitation. Geophys Res Lett 30:1241

Lawrence JE, Hornberger GM (2007) Soil moisture variability across climate zones. Geophys Res Lett 34:L20402

Lenschow DH, Mann J, Kristensen L (1994) How long is long enough when measuring fluxes and other turbulence statistics. J Atmos Ocean Technol 11:661–673

Malek E (2003) Microclimate of a desert playa: evaluation of annual radiation, energy, and water budgets components. Int J Climatol 23:333–345

Malek E, Bingham GE, McCurdy GD (1990) Evapotranspiration from the margin and moist playa of a closed desert valley. J Hydrol 120:15–43

Massey JD, Steenburgh WJ, Hoch SW, Knievel JC (2014) Sensitivity of near-surface temperature forecasts to soil properties over a sparsely vegetated dryland region. J Appl Meteorol Climatol 53:1976–1995

McCumber MC (1980) Numerical simulation of the influence of heat and moisture fluxes upon mesoscale circulations. PhD Thesis, University of Virginia

Menenti M (1984) Physical aspects and determination of evaporation in deserts applying remote sensing techniques. PhD Thesis, Netherlands Agricultural University

Mittelbach H, Seneviratne SI (2012) A new perspective on the spatio-temporal variability of soil moisture: temporal dynamics versus time-invariant contributions. Hydrol Earth Syst Sci 16:2169–2179

Novick KA, Oren R, Stoy PC, Siqueira MBS, Katul GG (2009) Nocturnal evapotranspiration in eddy-covariance records from three co-located ecosystems in the Southeastern U.S.: implications for annual fluxes. Agric For Meteorol 149:1491–1504

Oishi aC, Oren R, Stoy PC (2008) Estimating components of forest evapotranspiration: a footprint approach for scaling sap flux measurements. Agric For Meteorol 148:1719–1732

Ookouchi Y, Segal M, Kessler RC, Pielke RA (1984) Evaluation of soil moisture effects on the generation and modification of mesoscale circulations. Mon Weather Rev 112:2281–2292

Owe M, Jones EB, Schmugge TJ (1982) Soil moisture variation patterns observed in hand county, South Dakota. J Am Water Resour Assoc 18:949–954

Parlange MB, Katul GG, Cuenca RH, Kavvas ML, Nielsen DR, Mata M (1992) Physical basis for a time series model of soil water content. Water Resour Res 28:2437–2446

Philip JR (1957) Evaporation, and moisture and heat fields in the soil. J Meteorol 14:354–366

Priestley CHB, Taylor RJ (1972) On the assessment of surface heat flux and evaporation using large-scale parameters. Mon Weather Rev 100:81–92

Rife DL, Warner TT, Chen F, Astling EG (2002) Mechanisms for diurnal boundary layer circulations in the Great Basin Desert. Mon Weather Rev 130:921–938

Scanlon BR, Goldsmith RS (1997) Field study of spatial variability in unsaturated flow beneath and adjacent to playas. Water Resour Res 33:2239–2252

Schär C, Lüthi D, Beyerle U, Heise E (1999) The soil-precipitation feedback: a process study with a regional climate model. J Clim 12:722–741

Segal M, Garratt JR, Kallos G, Pielke RA (1989) The impact of wet soil and canopy temperatures on daytime boundary-layer growth. J Atmos Sci 46:3673–3684

Seneviratne SI, Corti T, Davin EL, Hirschi M, Jaeger EB, Lehner I, Orlowsky B, Teuling AJ (2010) Investigating soil moisture–climate interactions in a changing climate: a review. Earth Sci Rev 99:125–161

Shingleton N (2010) Coupling a land-surface model to large-eddy simulation to study the nocturnal boundary layer. MSc Thesis, The University of Utah
Soil Survey Staff (1999) Soil taxonomy: a basic system of soil classification for making and interpreting soil surveys. Agricultural handbook 438; Natural Resources Conservation Service, USDA, Washington DC, USA, 869 pp
Teuling AJ (2005) Improved understanding of soil moisture variability dynamics. Geophys Res Lett 32:L05404
Teuling AJ, Seneviratne SI, Williams C, Troch PA (2006) Observed timescales of evapotranspiration response to soil moisture. Geophys Res Lett 33:L23403
Teuling AJ, Hupet F, Uijlenhoet R, Troch PA (2007) Climate variability effects on spatial soil moisture dynamics. Geophys Res Lett 34:L06406
Tukey JW (1958) Bias and confidence in not-quite large samples. Ann Math Stat 29:614
Tyler SW, Muñoz JF, Wood WW (2006) The response of playa and sabkha hydraulics and mineralogy to climate forcing. Ground Water 44:329–38
USDA (1999) Soil quality test kit guide. USDA, Washington DC, USA, 82 pp
Vivoni ER, Gebremichael M, Watts CJ, Bindlish R, Jackson TJ (2008) Comparison of ground-based and remotely-sensed surface soil moisture estimates over complex terrain during SMEX04. Remote Sens Environ 112:314–325
Vivoni ER, Rodríguez JC, Watts CJ (2010) On the spatiotemporal variability of soil moisture and evapotranspiration in a mountainous basin within the North American monsoon region. Water Resour Res 46:W02509
Warner TT (2004) Desert meteorology. Cambridge University Press, Cambridge, 595pp
Western AW, Grayson RB (1998) The Tarrawarra data set: soil moisture patterns, soil characteristics, and hydrological flux measurements. Water Resour Res 34:2765–2768
Whitaker M (1993) Small-scale spatial variability of soil moisture and hydraulic conductivity in a semi-arid rangeland soil in Arizona. MS Thesis, The University of Arizona
Williams AG, Ternan JL, Fitzjohn C, de Alba S, Perez-Gonzalez A (2003) Soil moisture variability and land use in a seasonally arid environment. Hydrol Process 17:225–235
Williams CA, Albertson JD (2004) Soil moisture controls on canopy-scale water and carbon fluxes in an African savanna. Water Resour Res 40:W09302
Yechieli Y, Wood WW (2002) Hydrogeologic processes in saline systems: playas, sabkhas, and saline lakes. Earth Sci Rev 58:343–365
Yeh TCJ, Gelhar LW, Gutjar GAL (1985) Stochastic analysis of unsaturated flow in heterogeneous soils: 3. Observations and applications. Water Resour Res 21:465–471
Zheng X, Eltahir E (1998) A soil moisture-rainfall feedback mechanism 2. Numerical experiments. Water Resour Res 34:777–785
Zhou X, Geerts B (2013) The influence of soil moisture on the planetary boundary layer and on cumulus convection over an isolated mountain. Part I: observations. Mon Weather Rev 141:1061–1078